Anisotropic composite polymer for high magnetic force in microfluidic systems

A.-L. Deman, S. Mekkaoui, D. Dhungana, J.-F. Chateaux, A. Tamion, J. Degouttes, V. Dupuis, D. Le Roy

Anisotropic composite polymer for high magnetic force in microfluidic systems

A-L. Deman[1], S. Mekkaoui[1], D. Dhungana[1], J-F Chateaux[1], A. Tamion[2], J. Degouttes[1], V. Dupuis[2], D. Le Roy[2]

[1] *Univ Lyon, Université Claude Bernard Lyon 1, CNRS, Institut des Nanotechnologies de Lyon, INL-UMR 5270, F-69622, LYON, France*
[2] *Univ Lyon, Université Claude Bernard Lyon 1, CNRS, Institut Lumière Matière, F-69622, LYON, France*

corresponding author: *A.-L. Deman, anne-laure.deman@univ-lyon1.fr*

Abstract:

Anisotropic carbonyl iron-PolyDiMethylSiloxane (PDMS) composites were developed and implemented in microfluidic devices to serve as magnetic flux concentrators. These original materials provide technological solutions for heterogeneous integration with PDMS. Besides microfabrication advantages, they offer interesting modular magnetic properties. Applying an external magnetic field during the PDMS reticulation leads to the formation of 1D-agglomerates of magnetic particles, organized in the non-magnetic polymer matrix. This induces an increase of susceptibility as compared to composites with randomly dispersed particles. In this report, we explored the gain in reachable magnetophoretic forces in operating microfluidic devices, from the study of magnetic micro-beads motion injected in the microchannel. We show that even at relatively large distances from the magnetically-functionalized channel wall, the anisotropic composite leads to a factor two increase in the magnetophoretic force. Finally, further investigations based on finite element description suggest that the measured benefit of anisotropic composite polymers does not only rely on the global susceptibility increase but also on the local magnetic field gradients originating from the microstructure.

Keywords: magnetophoretic force, magnetic anisotropy, composite polymer, microstructuration/local magnetic gradients.

1 Introduction

Magnetophoresis, which refers to the motion of an object in a magnetic field gradient (Pamme 2006), is of great interest for the development of microsystems, notably for biomedical applications (Tekin and Gijs 2013, Moore et al. 2013, Phurimsak et al. 2014, Plouffe et al. 2015, Wu et al. 2016, Lee et al. 2017, Zhu et al. 2016). As compared to permanent magnets (Dumas-Bouchiat et al. 2010, Le Roy et al. 2016b), the use of soft magnetic structures that concentrate the flux of an external field offers the possibility to modulate or even cancelling the magnetic force to release on demand the trapped objects (Pamme 2006). For high concentration of magnetic flux, the soft magnetic structure should combine a large magnetization and preferentially a high effective magnetic susceptibility χ_{eff}, to operate at relatively low magnetic fields, while maintaining no hysteresis losses. Moreover, a way to improve experienced magnetic forces is to pattern the soft magnetic structures at the size of the channel that is in the submillimeter range (Yu et al. 2013, Esmaeilsabzali et al. 2016). To overcome the technological challenges owing to heterogeneous integration of metallic material with PolyDiMethylSiloxane (PDMS), as well as limitations related to pure metals micropatterning using time consuming, costly and complex UV-LIGA process (Esmaeilsabzali et al. 2016, Jung et al 2010), the approach of PDMS-based composite is promising (Faivre et al. 2014; Yu et al. 2014; Deman et al. 2011; Zhou et al. 2016a; Zhou et al. 2016b; Royet et al. 2016). The first benefit is that the composite preserves some PDMS properties such as soft-lithography micropatterning and O_2 surface activation for plasma bonding with glass and PDMS. In addition, the composite can be directly integrated into microchannels avoiding cumbersome alignment procedure. In a previous work, we succeeded in the realization of microfluidic devices integrating Carbonyl Iron - PDMS (I-PDMS) patterns and tested their ability to manipulate magnetic microbeads and magnetically labeled cells (Faivre et al. 2014). We recently reported on the possibility to form 1D-agglomerates of Carbonyl Iron particles in the composite applying a homogeneous magnetic field during the I-PDMS reticulation (Le Roy et al. 2016a). This induces a uniaxial magnetic anisotropy that was assessed by susceptibility measurements, over a large range of compositions, from 10 to 83wt%. The anisotropy was found to be more pronounced at low compositions, where the 1D-agglomerates were the most separated. However, this is at expense of the overall composite magnetization. At 83%, the saturation magnetization is of 650 kA/m, and the induced uniaxial anisotropy remains significant, with a nearly 20% increase in the susceptibility.

To go further, we have implemented such anisotropic I-PDMS in microfluidic system to study the gain in magnetophoretic performances as compared to isotropic I-PDMS. We measured the forces experienced by model micro-beads. The developed approach presented here permits to map magnetic field gradients, by analyzing microbeads trajectories when attracted to the microchannel wall made of I-PDMS. We show that the sole composite susceptibility change fails to describe the force variation across the channel. We discuss the effect of the fine microstructure using finite element analysis.

2 Microfabrication technology

2.1 Composite preparation

The composite polymer is obtained by mixing carbonyl iron microparticles (dry powder, 0.5-6 µm diameter, 97% Fe basis) (Sigma-Aldrich) and PDMS mixture (10/1 w/w of monomer and curing agent, respectively) (Sylgard from Samaro) in a mortar (around 4 min) until obtaining a homogeneous material. In this study, the carbonyl iron concentration is fixed to 83w%. For polymer reticulation step, the composite was either directly

baked at 75°C for 60 min, or submitted to a 130 mT uniform magnetic field for at least 12 hours before baking at 75°C for 60 min, to obtain respectively isotropic or anisotropic composite microstructures. The uniform field was created in the gap of two bulk permanent magnets. The magnetic field generated by the magnets was measured using a teslameter. Samples were precisely positioned at the middle of the gap where the magnetic field gradient was inferior to 0.1 T/m.

Fig. 1 (a,b) shows in plane views of both batches of composites. In the absence of magnetic field during the composite preparation, the dispersion of the carbonyl iron particles within the polymer matrix is homogenous (Fig. 1 (a)). In contrast, when the composite is prepared under magnetic field, the formation of 1D-shape agglomerates can be clearly seen along the magnetic flux lines through the overall composite film dimension (Fig. 1 (b)). At 83wt%, which corresponds to 38% in volume, the large amount of carbonyl iron particles gives rise to a dense composite with ramified and aligned chains.

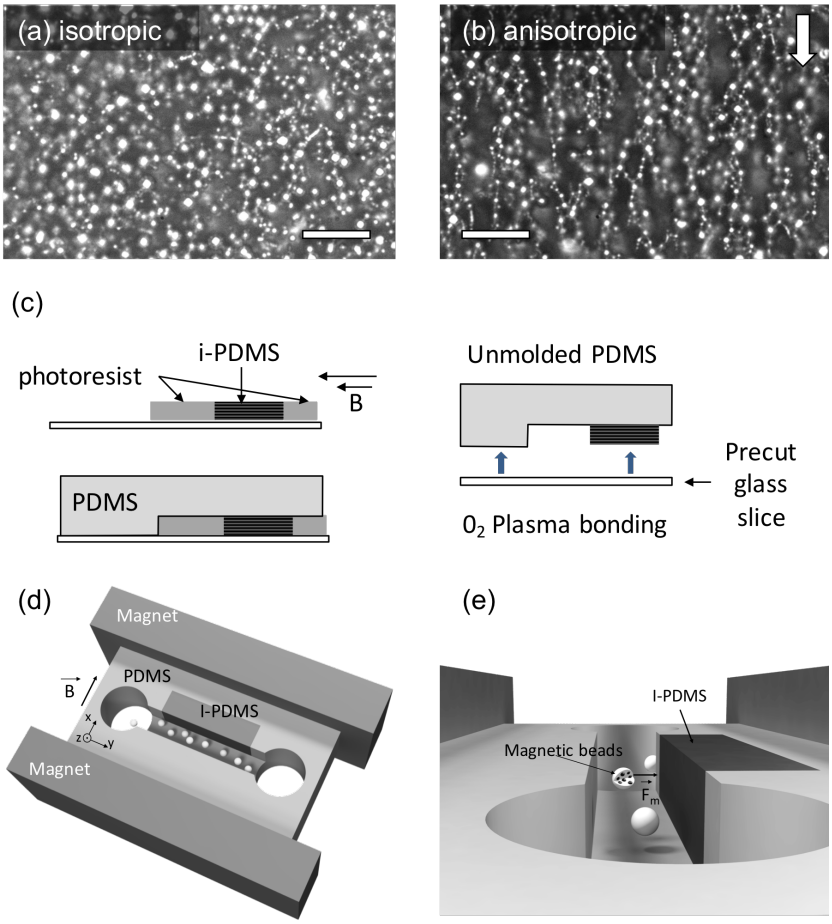

Fig. 1: Optical images of 83 wt% isotropic (a) and anisotropic (b) composite. The arrow indicates direction of the applied field during composite reticulation. The scale bar is 10 µm. Micro-system fabrication steps (c). Schematic of the microfluidic system that integrates I-PDMS structure on one side of the channel (d) and of the magnetic force experienced by magnetic beads in the channel (e).

2.2 Microfluidic device fabrication

We prepared microfluidic devices using soft lithography approaches based on the replication of masters. The

micro-channel molds were fabricated using dry 50 µm thick photoresist (Ethertec ®). The replication was obtained after a two steps process. In a first step, as shown on Fig. 1(c), the composite was poured between the channel mold and a stepper, the excess of magnetic polymer being removed with a blade. The obtained structures of i-PDMS were 50 µm thick (height of the channel, z direction), 2 mm wide (x direction) and 2 cm long (y direction). The composite was submitted or not to an external magnetic field of 130 mT, applied along the x direction, and baked as described previously. In a second step, we poured pure PDMS to mold the channel and baked the whole system at 75 °C for two hours. After PDMS unmolding, the channel was bonded to a glass slice, precut to fit in the Plexiglas frame used for microfluidic experiment. The obtained device was a single microfluidic channel, 1 mm width and 50 µm thick, with one wall made of magnetic composite, directly in contact with the circulating sample (Fig. 1 (d,e)).

2.3 Materials and experimental set-up

Superparamagnetic microbeads (magnetite nano-inclusions in polystyrene bead, Kisker ® with 12 µm in average diameter) were suspended, in deionized water and glycerol 50wt% (resulting viscosity, η = 6 mPa.s) with a concentration of 750 beads/µL. Glycerol was used to increase solution viscosity to facilitate videomicroscopic characterizations. During the experiment, a Plexiglas® holder, that integrates two permanent magnets (NdFeB 30x10x5mm^3, B_r of 1.2 T, polarization in the shortest dimension), was used to precisely position the microfluidic system. The microchannel is thus localized in the middle of the gap of 11 mm separating the two magnets, where the magnetic field has been measured at 143 kA/m, using a teslameter. As the Hall sensor of the teslameter is relatively large, about 1 mm^2 section, we simulated the set-up using COMSOL Multiphysics 4.2a ®, and calculated generated magnetic field profile throughout the channel section. Both measurements and simulations were consistent and confirmed the uniformity of the applied field in the channel, with gradients of less than 0.1 T/m. The bead motions were recorded using an inverted fluorescence microscope (Leica DMI4000B) mounted with a camera (Leica DFC340 FX). Images were recorded with an average time interval of 640 ms. Bead coordinates for all images were obtained using MTrackJ ImageJ® plugin.

3. Theory and method

In the microchannel, the superparamagnetic beads are submitted to different forces: (i) magnetophoretic force $\vec{F}_m$, (ii) fluidic drag force $\vec{F}_d$, (iii) gravitational force $\vec{F}_g$, and (iv) buoyancy forces $\vec{F}_{buo}$. Other forces describing bead-bead interactions, fluid-bead interactions, van der Waals attraction force, Brownian forces are neglected due to the low concentration of beads in the solution and to their microsize. Classical physics is then employed to describe the beads trajectory (Furlani 2010). According to the Newton's second law, motion of a magnetic bead in a laminar flow can be determined by the balance of forces:

$$m_b \frac{\mathrm{d}\vec{v}_b}{\mathrm{d}t} = \vec{F}_m + \vec{F}_d + \vec{F}_g + \vec{F}_{buo} \qquad (1)$$

m_b being the mass of the bead and $\vec{v}_b$ its velocity. Generally, the inertial term and gravitational and buoyancy forces are neglected. Indeed, for sub-micrometer size beads, the inertial term, $m_b \frac{dv_b}{dt}$, is often ignored due to small mass of these beads, and the gravitational and buoyancy forces are generally found one or two orders of magnitude lower than the magnetic and the drag force. For larger beads or cells these terms may need to be included. In the following section, they will be estimated in the particular case of our study.

The magnetic force experienced by a magnetic bead in a non-magnetic fluid and submitted to an applied field H_a is:

$$\vec{F}_m = \mu_0 V_b (\vec{M}_b \cdot \vec{\nabla}) \vec{H}_a \qquad (2)$$

V_b being the volume of the bead, M_b its magnetization, which can be expressed as $\vec{M}_b = f(H_a)\overrightarrow{H_a}$.

In the equation (2), we assume that the bead is uniformly magnetized (Hejazian et al. 2014, Pamme 2006). In our case, the beads motion is studied at relatively larges distances from the source of magnetic field gradient (150 µm to 250 µm), where the variation of H_a is inferior to 0.5 mT over the beads diameter (12 µm). At low magnetic field, i.e. when $M_b << M_s$ (with M_s the saturation magnetization of the beads), M_b varies linearly with H_a and therefore the force scales with $(\overrightarrow{H_a} \cdot \vec{\nabla})\overrightarrow{H_a}$. In contrast, at relatively high field, the magnetization is independent to H_a and the force then scales with $\vec{\nabla}\,\overrightarrow{H_a}$.

We measured the beads magnetization in a SQUID magnetometer in order to determine if they were saturated or not regarding our experimental set-up. Beads presented a superparamagnetic behavior, which is characterized by two main regimes. At relatively low field, the magnetization varies nearly linearly with the field and the susceptibility is maximum. At high enough field, the magnetization reaches saturation. In between, the non-linear response implies to use a Langevin function [Zhu et al. 2011, Cheng et al. 2014). In agreement with the supplier description, the magnetization curve of the beads was well described by a Langevin function of an ensemble of Fe_3O_4 nanoparticles (8.4 nm diameter) embedded in the non magnetic polystyrene matrix. The susceptibility was found to be linear in a relatively small range of field close to zero, as the first derivative $\frac{\Delta M}{\mu_0 M_S \Delta H_a}$ was divided by two when the field increased from 0 to 55mT. In the channel, the minimum magnetic field seen by the beads was Ha = 143 kA/m (*i.e.* μ_0Ha = 180 mT), thus relatively far from the linear regime. Indeed, above 180 mT, the magnetization was larger than 85%Ms, and was almost constant in the region of the channel we considered in the following discussion (magnetization variation of 1%Ms over 10 mT). Therefore, we assumed the magnetization of the beads as saturated, and magnetic forces scaling with $\vec{\nabla}\,\overrightarrow{H_a}$.

The drag force is expressed as follows:

$$\vec{F}_d = 6\pi\eta R_b (\vec{v}_f - \vec{v}_b) f_D \qquad (4)$$

R_b being the radius of the bead, η and v_f respectively the viscosity and the velocity of the solution. f_D is the drag coefficient of the particle that accounts for the influence of a solid wall in the vicinity of the particle, and z is the distance of the particle to the wall (Gijs et al. 2010).

$$f_D = \left[1 - \frac{9}{16}\left(\frac{R_b}{R_b + z}\right) + \frac{1}{8}\left(\frac{R_b}{R_b + z}\right)^3 - \frac{45}{256}\left(\frac{R_b}{R_b + z}\right)^4 - \frac{1}{16}\left(\frac{R_b}{R_b + z}\right)^5\right]^{-1} \qquad (5)$$

The sum of the gravitational force and the buoyancy force are expressed as follow:

$$\vec{F}_g + \vec{F}_{buo} = -V_b\left(\rho_b - \rho_f\right)\vec{g} \qquad (6)$$

with ρ_b and ρ_f the density of the bead and the solution, respectively, and g the acceleration due to gravity.

The balance of forces can then be written as:

$$m_b \frac{\mathrm{d}\vec{v}_b}{\mathrm{d}t} = \mu_0 V_b M_S \vec{\nabla}\vec{H}_a + 6\pi\eta R_b(\vec{v}_f - \vec{v}_b) f_D - V_b\left(\rho_b - \rho_f\right)\vec{g} \qquad (7)$$

The method used to map magnetophoretic force experienced by the beads in the channel is the following. The channel was first filled up with beads while the initial position of the beads in the channel is defined by stopping the flow rate ($\boldsymbol{v_f} = 0$). The Plexiglas® holder, that integrates two permanent magnets, was then positioned over the microchannel. Submitted to a magnetic field gradient, the superparamagnetic beads were attracted toward the I-PDMS composite wall of the channel. Fig. 2 displays a stacking of video frames revealing microbeads trajectories. This method, performed directly on chip, was inspired by the one developed by C. Wilhelm et al. (2002) to quantify magnetic labelling of cells. From the beads velocities and accelerations, we could estimate the different forces contributions and map the magnetophoretic force across the channel.

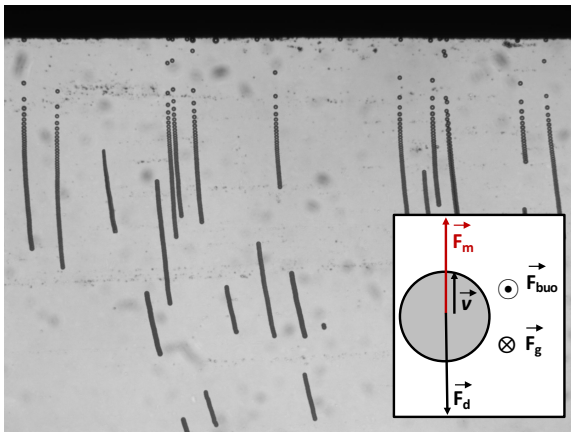

Fig. 2: Z-stack projection of videomicroscopic images representing superparamagnetic particles moving toward the composite wall of the microsystem. Inset: Schematic of forces experienced by microbeads in the microchannel.

4 Results and discussion

The main objective of this work is to demonstrate the interest of conferring anisotropic magnetic properties to I-PDMS to implement magnetophoretic functions in microdevices. We studied beads motion in order to estimate forces involved, and map the magnetophoretic force in the microchannel. We discussed phenomena that contribute to magnetophoretic force gain such as global susceptibility increase, and local magnetic field gradients originating from the composite fine periodic microstructure.

4.1 Balance of forces

As expected, the magnetic flux concentration by the composite produced a region of maximum field on one side of the microfluidic channel, which attracts the injected beads. We compared the bead trajectories in microfluidic system that integrate anisotropic and isotropic composites. Fig. 3 displays the displacement recorded during 640 ms, at a distance of 200 +/- 10 µm from the wall. The displacement was found to be two times larger in the case of anisotropic composite than in the case of isotropic composite, with an average travelled distance of 24 µm and 12.3 µm, respectively. From videomicroscopic observations, we recorded the time-dependence of the bead positions and determined the bead velocities and accelerations as a function of their distance from the wall. Calculated acceleration at a distance of 200 +/- 10 µm from the wall is shown in the inset of Fig. 3. At a distance of 200 µm from the wall, we obtained an average acceleration of 22 µm/s^2 and 7.5 µm/s^2 for anisotropic and isotropic composites, respectively. This shows that even at relatively large distance to the wall, anisotropic I-PDMS remains more efficient.

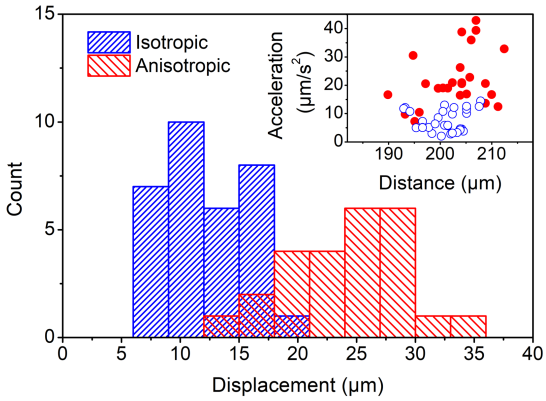

Fig. 3: Histogram of the measured bead displacements towards anisotropic (red) or isotropic (blue) composite-constituted wall, at a distance of 200 µm +/-10µm from the wall and during an interval of time of 640 ms. The inset shows the bead accelerations at the same distance from the wall: red circles and blue squares, for respectively, anisotropic and isotropic microstructures.

Accordingly, one can estimate that inertial term of equation (1) amounts from 7.5 10^{-3} to 2.2 10^{-2} pN. Beads and liquid density being respectively of 1100 kg/m^3, and 1130 kg/m^3, sum of F_g and F_{buo} is in the order of 0.3 pN magnitude. We obtained velocities values ranging from 5 to 80 µm/s. Considering a channel thickness of 50 µm,

average beads radius of 6 µm and minimum f_D of 1.15, the drag force F_d values reach tens of pN. Inertial term, gravitational and buoyancy forces were then neglected. Thus equation (7) can be reduced to:

$$\vec{F}_m = \mu_0 V_b M_S \vec{\nabla} \vec{H}_a = 6\pi\eta R_b \vec{v}_b f_D \qquad (8)$$

4.2 Magnetophoretic force mapping

Based on equation 8, the magnetophoretic force experienced by microbeads in the channel is proportional to their velocities, as recorded by videomicroscopy. Fig. 4 shows the deduced F_m at different distances from the composite wall, i.e., 150 µm, 200 µm and 250 µm.

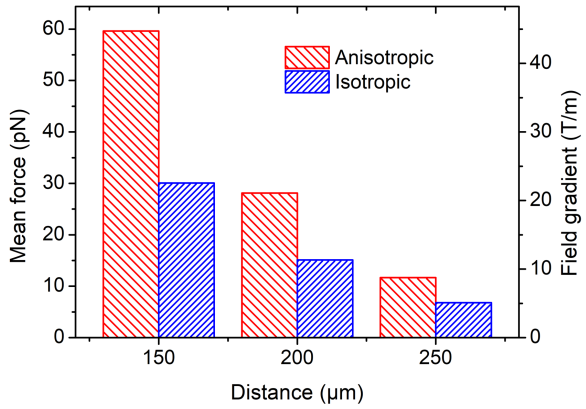

Fig. 4: Mean magnetic force generated by anisotropic (red, left bars) or isotropic (blue, right bars) composite microconcentrators at distances of 150µm, 200 µm and 250 µm form the composite. The right Y-axis shows the corresponding value of field gradient.

The magnetic force increased when approaching the composite wall depicting the expected field gradient profile. The magnetic force experienced by microbeads reached 60 pN at a distance of 150 µm when using anisotropic composite while it was about 30 pN with isotropic composite. The field gradient values at the same distance were of 44 T/m and 22 T/m, respectively. This large difference of magnetic force contrasts with the relatively small magnetization difference of 16% measured between the anisotropic and isotropic composites at 143 kA/m (Le Roy et al. 2016). In addition, as shown in Fig. 5, the ratio of anisotropic to isotropic composite magnetic gradient was not constant and increased from 1.7 at a distance of 250 µm from the composite to 2 at a distance of 150 µm. Approaching the wall, forces generated using anisotropic composite increased more significantly. Thus, we used finite elements simulation to describe both the influence of the composite magnetic susceptibility and its microstructure on the produced local magnetic field gradients. We performed 2D simulations, in X-Z plane (the plane containing the channel section), using COMSOL Multiphysics 4.2a ®, according to our experimental set-up geometry. As a reminder, it consisted of two face-to-face permanent magnets (5x10 mm^2), placed in attraction and separated by 11 mm gap. The channel section (1000x50μm^2), considering a composite wall (200x50μm^2), was placed in the middle of the gap. The relative permeability was set as $\mu_r = 1$ except in the

magnets and in the composite material. For non-linear permanent magnet, we considered its remanent magnetic induction B_r (1.17 T) and a relative permeability (μ_r) of 1.05. Concerning the composite wall, we developed two different models to account for the composite magnetization and its microstructure. In the first model (Fig. 5, configurations A and B) based on SQUID results, we considered a difference in the relative permeability with μ_r = 4,35 for the isotropic composite (A), and $\mu_{r,x}$ = 5,22 and $\mu_{r,z}$ = 4,45 for the anisotropic composite (B). Under the microdevice operating conditions, at a distance of 150 to 250 µm from the wall, the calculated force ratio, denoted B/A on Fig. 5, is slightly lower than the one experimentally measured and remains nearly constant over the range of considered distances. By increasing $\mu_{r,x}$ up to 8, the experimental force ratio of 1.7 was achieved, but remained constant over distances of 250 µm to 150µm to the composite pattern. Anisotropic magnetization of the composite improves magnetic flux concentration but it does not explain the increase of the magnetic field gradient created by the composite pattern. In the second model, in order to take into account the composite microstructures, we considered and compared two designs: (i) microstructure of a checkerboard composed of alternating particles (black) and pure PDMS areas of 2 µm in size (average size of carbonyl iron particles), to model isotropic composite, (ii) 1D microstructure of lines, 2 µm wide, alternating particles and pure PDMS, as illustrated in D, to model anisotropic composite. The calculated force ratio, denoted D/C, also reported on Fig. 5, is slightly superior to the experimental one, but qualitatively reproduces the tendency to increase when approaching the composite. The generated forces obtained using composite microstructured in lines increased more significantly than the ones obtained with checkerboard microstructure. Local gradients generated by line structure composite, modeling particle ordering in chains in the composite matrix, participate in magnetic forces, even at distance of 150 to 250 µm. These findings reinforce assumption that, beyond the susceptibility change, the microstructure of the composite contribute to the created magnetic flux and as a result on the magnetophoretic force experienced by magnetic beads flowing in the channel.

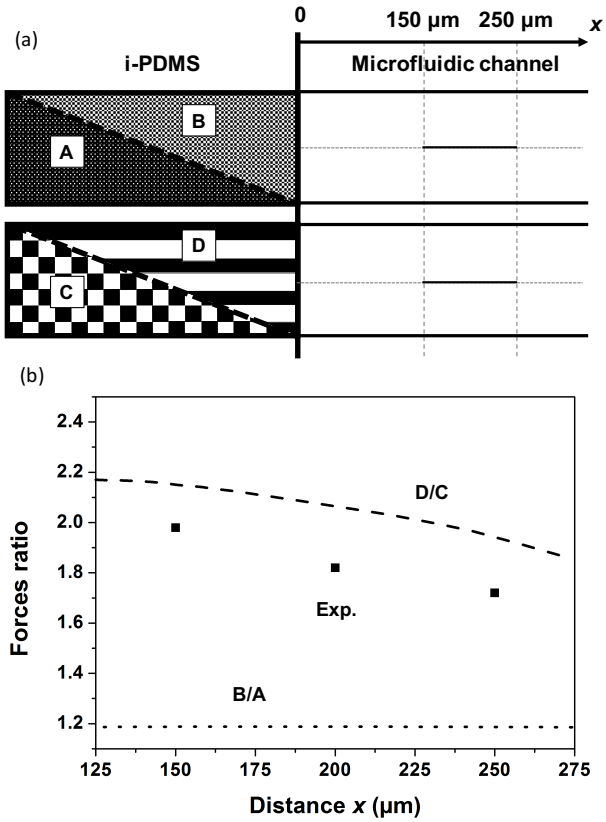

Fig. 5: Influence of susceptibility and structuration of i-PDMS composite on the magnetphoretic force in the fluidic microchannel. (a) Schematics of the considered i-PDMS microstructures. (b) Corresponding forces ratio considering anisotropic and isotropic i-PDMS, at 125 µm to 275 µm distance from the wall: solid squares represent experimental values, the dashed and dotted lines are obtained from simulation of cases B/A and D/C, respectively.

5. Conclusion

We have demonstrated interest of using anisotropic I-PDMS to implement magnetophoretic functions in microfluidic systems. Here we compared devices integrating either anisotropic or isotropic I-PDMS. We studied microbead trajectories towards the magnetically functionalized wall. The estimation of all involved forces pointed out that only the drag force and the magnetophoretic force governed the system, which leads to a simplified relationship between the beads motion and the magnetophoretic force. In addition, operating at relatively large external field, we could limit the discussion to the case of magnetization-saturated beads, where the magnetic force scales with $\vec{\nabla}\,\overrightarrow{H_a}$. At a distance of 150 µm form the microconcentrator, we measured a force reaching 60 pN using the anisotropic I-PDMS, a force twice as large as the one measured using isotropic composite. From the measured variation of the magnetophoretic forces across the channel and finite element simulations, we highlighted that the benefit of using anisotropic composite does not only rely on the global susceptibility increase, but also on local magnetic field gradients originating from its fine periodic microstructure. Anisotropic I-PDMS is a promising material in the general context of microfluidic devices, in particular regarding the keen interest for lab on a chip dedicated to personalized medicine.

Acknowledgments

The authors are indebted to the EEA doctoral school and the institute Carnot Ingénierie@Lyon, and for their support and funding. This work was also supported by the University of Lyon 1, through its program «BQR Accueil EC 2015 ». The authors are grateful to R. Checa for technical assistance at the « Centre de Magnétométrie de Lyon », and to N. Terrier for his technical support at the NanoLyon cleanroom facility.

References

- Cheng R, Zhu T, Mao L (2014) Three-dimensional and analytical modeling of microfluidic particle transport in magnetic fluids. Microfluid. Nanofluid. 16, 1143
- Dumas-Bouchiat F, Zanini LF, Kustov M, Dempsey NM, Grechishkin G, Hasselbach K, Orlianges JC, Champeaux C, Catherinot A, Givord G (2010) Thermomagnetically patterned micromagnets. Appl. Phys. Lett. 96, 102511.
- Esmaeilsabzali H, Beischlag TV, Cox ME, Dechev N, Parameswaran AM, Park AJ (2016) An integrated microfluidic chip for immunomagnetic detection and isolation of rare prostate cancer cells from blood. Biomed. Microdev. 18:22Faivre M, Gelszinnis R, Degouttes J, Terrier N, Rivière C, Ferrigno R, Deman AL (2014) Magnetophoretic manipulation in microsystem using carbonyl ironpolydimethylsiloxane microstructures. Biomicrofluidics 8, 054103.
- Furlani EP (2010) Magnetic Biotransport: Analysis and Applications. Materials 3, 2412-2446.
- Gijs MAM, Lacharme F, Lehmann U (2010) Microfluidic applications of magnetic particles for biological analysis and catalysis. Chem. Rev. 110, 1518-1563.
- Hejazian M, Li W, Nguyen N.-T. (2015) Lab on a chip for continuous-flow magnetic cell separation, Lab Chip, 15, 959
- Jung Y, Choi Y, Han KH, Frazier AB (2010) Six-stage cascade paramagnetic mode magnetophoretic separation system for human blood samples. Biomed Microdev. 12, 637-645.
- Lee TY, Hyun KA, Kim SI, Jung H (2017) An integrated microfluidic chip for one-step isolation of circulating tumor cells. Sensors and Actuators B: Chemical 238: 1144-1150.
- Le Roy D, Dhungana D, Ourry L, Faivre M, Ferrigno R, Tamion A, Dupuis V, Deman AL (2016) Anisotropic ferromagnetic polymer: A first step for their implementation in microfluidic systems. AIP Advances 6, 056604.
- Le Roy D, Shaw G, Haettel R, Hasselbach K, Dumas-Bouchiat F, Givord D, Dempsey NM (2016) Fabrication and characterization of polymer membranes with integrated arrays of high performance micro-magnets. Materials Today Communications 6, 50-55.
- Moore LR, Nehl F, Dorn J, Chalmers JJ and Zborowski M (2013) Open Gradient Magnetic Red Blood Cell Sorter Evaluation on Model Cell Mixtures. IEEE Trans. Magn. 49: 309-315.
- Pamme N (2006) Magnetism and microfluidics. Lab Chip 6, 24-36.
- Phurimsak C, Tarn MD, Peyman SA, Greenman J and Pamme N (2014) On-Chip Determination of C-Reactive Protein Using Magnetic Particles in Continuous Flow. Anal. Chem. 86:10552-10559.
- Plouffe BD, Murthy SK, Lewis LH (2015) Fundamentals and application of magnetic particles in cell isolation and enrichment: a review. Rep. Prog. Phys. 78 016601.
- Royet D, Hériveaux Y, Marchalot J, Scorreti R, Dias A, Dempsey N M, Bonfilm M, Simonet P, Frenea-Robin M (2016) Using injection molding and reversible bonding for easy fabrication of magnetic cell trapping and sorting devices. J. Magn. Magn. Mater. http://dx.doi.org/10.1016/j.jmmm.2016.10.102
- Tekin HC and Gijs MAM (2013) Ultrasensitive protein detection: a case for microfluidic magnetic bead-based assays. Lab Chip DOI: 10.1039/c3lc50477h.
- Wilhelm C, Gazeau F, Bacri JC (2002) Magnetophoresis and ferromagnetic resonance of magnetically labeled cells. Eur. Biophys. J. 31, 118.
- Wu WT, Martin AB, Gandini A, Aubry N, Massoudi M and Antaki JF (2016) Design of microfluidic channels for magnetic separation of malaria-infected red blood cells. Microfluid. Nanofluid. 20:41.
- Yu X, Xia HS, Sun ZD, Wang K, Yu J, Tang H, Pang DW, Zhang ZL (2013) On-chip dual detection of cancer biomarkers directly in serum based on self-assembled magnetic bead patterns and quantum dots.

Biosensors and Bioelectronics. 41, 129-136.
- Yu X, Wen CY, Zhang ZL, Pang DW (2014) Control of magnetic field distribution by using nickel powder@PDMS pillars in microchannels. RCS Adv. 4, 17660.
- Zhou R, Wang C (2016)a Microfluidic separation of magnetic particles with soft magnetic microstructures. Microfluid. Nanofluid. 20:48
- Zhou R, Yang B, Bai F, Werner JA, Shi H, Ma Y, Wang C (2016)b Fabrication and integration of microscale permanent magnets for particle separation in microfluidics. Microfluid. Nanofluid. 20:110.
- Zhu Y, Kekalo K, Dong CN, Huang YY, Schubitidze F, Griwold KE, Baker I and Zhang JXJ (2016) Magnetic-Nanoparticle-Based Immunoassays-on-Chip: Materials Synthesis, Surface Functionalization, and Cancer Cell Screening. Adv. Funct. Mater. 26 22, pp. 3953-3972.
- Zhu T, Lichlyter D. J., Haidekker M. A, Mao L (2011) Analytical model of microfluidic transport of non-magnetic particles in ferrofluids under the influence of a permanent magnet. Microfluid. Nanofluid. 10, 1233